SSC-110

The Superconducting Super Collider

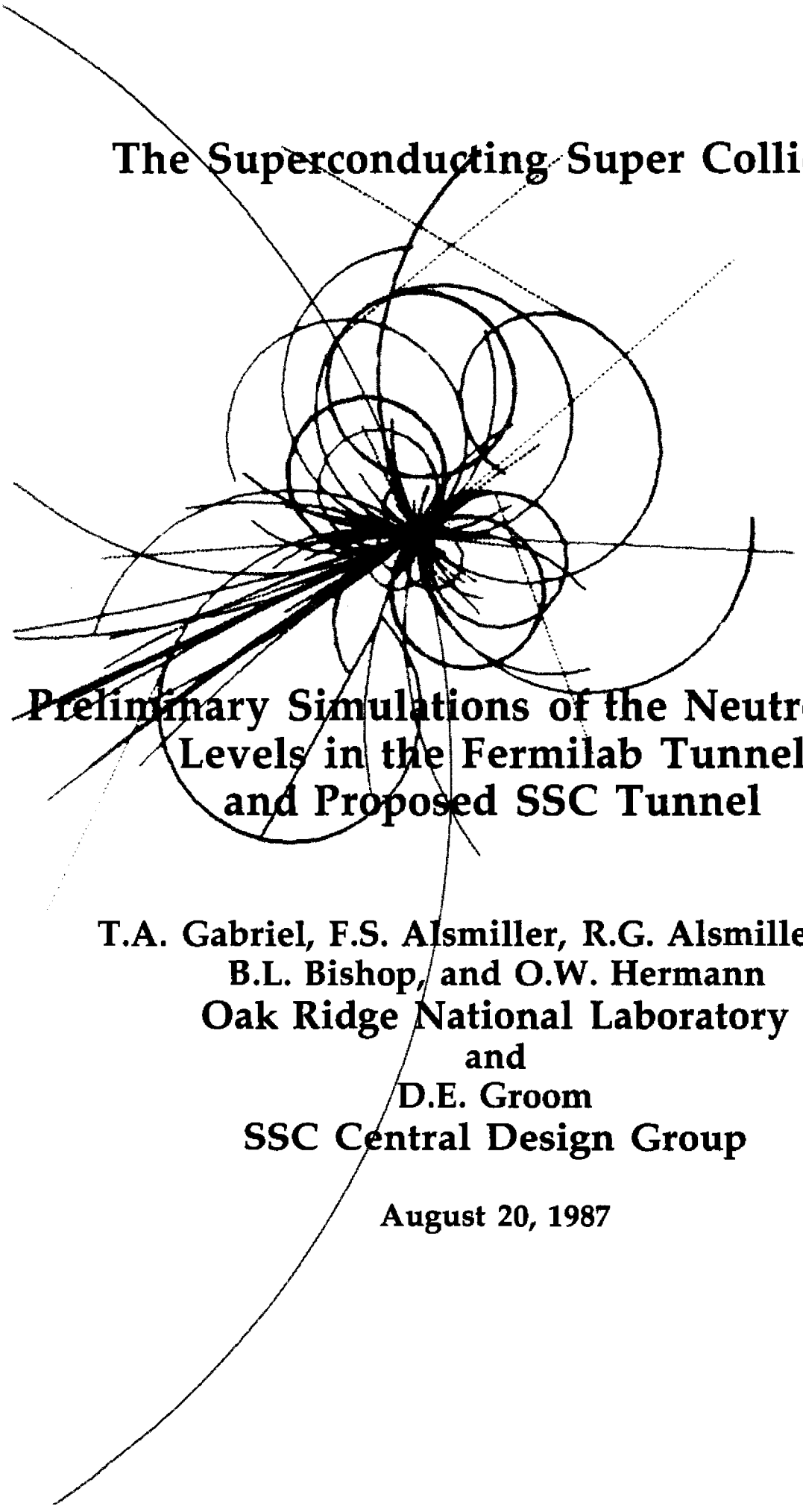

Preliminary Simulations of the Neutron Flux Levels in the Fermilab Tunnel and Proposed SSC Tunnel

T.A. Gabriel, F.S. Alsmiller, R.G. Alsmiller, Jr.,
B.L. Bishop, and O.W. Hermann
Oak Ridge National Laboratory
and
D.E. Groom
SSC Central Design Group

August 20, 1987

SSC-110

PRELIMINARY SIMULATIONS OF THE NEUTRON FLUX LEVELS IN THE FERMILAB TUNNEL AND PROPOSED SSC TUNNEL

T. A. Gabriel, F. S. Alsmiller

R. G. Alsmiller, Jr., B. L. Bishop, and O. W. Hermann

Oak Ridge National Laboratory, Oak Ridge TN 37830

and

D. E. Groom

SSC Central Design Group, c/o LBL, 1 Cyclotron Road, Berkeley CA 94720*

August 20, 1987

*Operated by Universities Research Association for the Department of Energy.

SSC-110
20 August 1987

Preliminary Simulations of the Neutron Flux Levels in the Fermilab Tunnel and Proposed SSC Tunnel

T. A. Gabriel, F. S. Alsmiller,
R. G. Alsmiller, Jr., B. L. Bishop, and O. W. Hermann
Oak Ridge National Laboratory, Oak Ridge TN 37830
and
D. E. Groom
SSC Central Design Group, LBL 90-4040, Berkeley CA 94720

1. Introduction

In the fall of 1985, a FNAL/LBL group measured neutron spectra in the Tevatron tunnel[1]. During the machine cycle just ended (early 1987), these experiments were refined and extended[2]. Absolute magnitude and longitudinal distributions of the neutron flux were measured down the tunnel from a warm section in the beam pipe. A controlled N_2 gas leak was introduced near the center of the warm section, so that by measuring rates as a function of gas pressure, beam-gas rates could be separated from background rates. To help support this experimental effort, detailed simulations of particle cascades in the Fermilab tunnel initialed by hadron-nucleus collisions ($E_p = 875$ GeV) in the center of the warm section were carried out using a version of HETC[3]. The MORSE code[4] was used to transport the low-energy (≤ 20 MeV) neutrons. In this note, preliminary results from these simulations are presented, as well as results calculated at SSC energies, i.e., at 20 TeV. The simulations will become more detailed as the experimental analysis proceeds, and the feedback obtained from the experiment will allow further improvements in the transport capabilities. Final reports detailing both calculational and experimental results will be published.

The study was motivated by concern about radiation damage to silicon semiconductors in the SSC tunnel. About 400 racks of control circuitry are located at 200 m intervals around the ring, and in addition a variety of temperature sensors, beam pickups, and perhaps quench protection diodes are mounted on or in each of the 10,000 magnets. The physics of radiation damage in silicon relevant to this study is discussed in Appendix 1.

2. Method

A modified three-dimensional high-energy hadron transport Monte Carlo code, HETC [3], is used to obtain a detailed description of the hadronic cascades in the Tevatron and SSC tunnels. For hadron-nucleus collisions with incident energy > 3 GeV, the multi-chain fragmentation model developed by Capella and Tran Tanh Van [5] and implemented by Ranft *et al.* in FLUKA82 [6] is used. This model has been further extended for use in HETC by the inclusion of an evaporation calculation so that low-energy neutron emission can be considered [7]. The inclusion of this model in HETC represents the only substantive difference between the modified HETC and that used previously (See Ref. 3 and the references given therein). In particular the intranuclear cascade evaporation model that is used to describe hadron-nucleus collisions below 3 GeV has been retained since results obtained with this model have previously been shown to agree with experimental data [8]. The Monte Carlo code MORSE was used to transport neutrons produced in HETC with energies below 20 MeV. Cross section data from MORSE were obtained from the VITAMIN-E data library [9] and contain 53 neutron energy groups.*

For the present calculations, approximately 3000 neutrons per 875 GeV proton and 30,000 neutrons per 20 TeV proton are produced in HETC for transport in the MORSE code. Fewer than 3% of these low-energy neutrons originate in collisions with hadrons of energy above 3 GeV.

The first MORSE runs were quite time-consuming since neutrons were transported until they were captured or escaped from the system. Since the main interest in these initial calculations is in damage to semiconductor electronics, the current cutoff on neutron energy has been set at 40 keV, i.e. neutrons with energies below 40 keV are not considered. As per the discussion in Appendix 1, neutrons with energies below about 160 keV are not effective in damaging silicon devices. Using the 40 keV cutoff has resulted in substantial savings in computer time.

Once the neutron flux has been calculated, parameters proportion to the damage ($\int_{E>0.1\ \mathrm{MeV}} \phi(E)dE$ or $\int \phi(E)\sigma_D dE$ (where σ_D is the displacement cross section) or $\int \phi(E)\sigma_{\mathrm{kerma}} dE$) can be calculated and compared with benchmark damage studies data [10] to determine if redesign or additional shielding of the electronics may be necessary.

---

* All the neutrons in each energy group (for example the 10th, between 9.05 and 10.0 MeV) are assumed to behave in the same way—they have the same transport cross section, the same absorption probability, scattering characteristics, etc.

3. Tevatron model

The Tevatron tunnel and magnet geometry have been described elsewhere [11], and are shown in Fig. 1, along with detector positions in the 1985 and 1986-87 experiments. Since HETC and MORSE utilize combinatorial geometry, any geometry can be constructed. However, for these preliminary scoping studies, cylindrical geometry was chosen. The real tunnel was replaced by the model shown in Figs. 2 and 3. In the calculations the neutron flux is obtained by scoring neutron track length in the volume shown by the cross-hatched region in Fig. 3, i.e. from $r_1 = 50$ cm to the tunnel wall at $r_2 = 152$ cm.

The main difference between the model and real Tevatron is that the "detector" is on the average closer to the source in the model. If the magnet string were a uniform line source of neutrons, the flux coming directly from the magnets (the "direct" flux) would fall off as $1/r$. The part of the flux due to scattering from the tunnel walls (the "albedo" flux) should be independent of position within the tunnel. The program scores neutron track length within each fiducial volume, and divides the total track length by the volume to find the average flux in the volume. For a cylindrical shell with inner and outer radii r_1 and r_2,

$$\frac{\text{Total track length}}{\pi(r_2^2 - r_1^2)} = \frac{\text{Total track length}/\Delta r}{2\pi(r_2 + r_1)/2} \ .$$

Since the total track length for the direct component is proportional to the cylinder thickness $\Delta r = r_2 - r_1$, the flux obtained is the same as that at a detector at the average radius $\langle r \rangle = (r_2 + r_1)/2$. In the Tevatron experiment, the detector was near the wall, about 200 cm from the magnet. Therefore the direct flux component must be scaled down by $50 + 152)/(2 \times 200) \approx 0.50$ to compare simulation results with experimental results.

The same result is obtained for a point neutron source and an infinitely long hollow cylindrical scoring volume. For a point source and a longitudinally segmented volume, flux in segments far away from the source is insensitive to radial thickness. For segments near the source, the scored direct flux is the actual direct flux at a radius smaller than the average. The exact scaling is geometry-dependent, and in practice it is easier to introduce further radial segmentation into the calculation.

The model assumes that the primary interactions occur in an iron "flying wire" at the origin. The debris from a collision goes mostly forward, and in the absence of a magnetic field in the dipole would stay in the beam pipe for an unrealistically long distance. A dipole field in the beam pipe is accordingly introduced ($B = 3.85$ T at 875 GeV, and 5.4 T at 20 TeV), while the field in the iron has so far been neglected.

In the experiment, collisions occur over the 12 m long warm section and not at a point. As a result, the calculated response as a function of distance is expected to be more sharply peaked than the experimental distribution.

Tunnel curvature has also been neglected. This will have the effect of letting neutrals propagate too far before encountering walls, or of extending longitudinal distributions. An on-axis neutron travels 8 m before striking a properly curved vacuum chamber wall, and if its average $p_\perp$ is 0.5 GeV/c this result is not substantially changed. However, this should not introduce large differences in the comparison between calculated and experimental data.

4. Results

Hadronic cascade calculations were carried out in late November, 1986, to check the code system. No cutoff energy was applied to the low-energy neutrons in these calculations. Additional boundaries in the geometry for the air section were added (finer binning in z), and, as described above, the threshold below which neutrons were not transported was increased to 40 keV. Four longer calculations were made in late December, 1986, and late January, 1987,* and are described in Table 1. Tunnel walls were "removed" in some runs in order to obtain the direct neutron flux, that is, the component resulting from particles produced in the dipoles but not scattering from the tunnel walls before passing through the fiducial volume. Given good enough statistics, the albedo flux can be obtained by subtraction.

Table 1

December 1986 ORNL simulations.

Run	Tevatron Energy	Conditions
1Y	875 GeV	Tunnel walls present
1N	875 GeV	Tunnel walls absent
20Y	20 TeV	Tunnel walls present
20N	20 TeV	Tunnel walls absent

* Originally, the z distributions were not extended beyond 30 m, or 22.7 m from the dipole entrance. While this was sufficient in the 875 GeV case, substantial flux occurred beyond this in the 20 TeV case. The 20 TeV calculations were repeated with the z distributions taken to 100 m.

Longitudinal (z) distributions of the total neutron flux above 40 keV and less than 20 MeV are shown in Figs. 4 and 5 for 875 GeV and 20 TeV, respectively. Collisions at $z = 0$ produce debris peaked in the forward direction, most of which enters the dipole aperture at 7.3 m. Charged particles are bent into the dipole yoke fairly quickly, where they initiate further cascades. Neutrals eventually hit the walls, at distances dependent upon their angles and the curve of the vacuum chamber.

The 875 GeV distribution shown in Fig. 4 peaks at about 8 m (about a meter past the entrance of the first dipole), then drops nearly exponentially, with the total flux falling off as $\exp(-z/4.4\text{ m})$. As expected, the albedo component has a somewhat broader distribution than the direct component. Also shown in this figure by the solid curve is the preliminary experimental distribution. It is considerably broader, and peaks at larger z. As mentioned above, the difference is very likely due to the fact that the experimental source is distributed over nearly 12 meters in the warm straight section. Simulations now in progress should shed more light on this subject.

In addition to the more extensive longitudinal distribution, the 20 TeV results show a long, flat tail composed almost entirely of albedo particles. While these contribute little to the integral, it is interesting to note that the exponential falloff evident in the 875 GeV case shown in Fig. 4 does not continue.

Suppose that a proton interacts at a point z' with probability dz'/C in a continuous magnet string, as will be the case for beam-gas collisions in the SSC. A detector at a point z, at a given distance from the magnet, measures a flux $f(z - z')dz'/C$. The total flux in the detector from uniformly distributed sources of this kind will then be

$$\begin{aligned}\phi &= \frac{1}{C}\int f(z - z')dz' \\ &= \frac{1}{C}\int f(z')dz'\end{aligned}$$

when the integral is carried out over all z' for which f is non-zero. In making the connection between the continuously distributed case and the localized distribution, it is thus the *integral* of the distribution which is relevant. The function $f(z)$ is somewhat different than the longitudinal distribution measured in the Tevatron experiment or calculated in the present simulation, where the source is in a long field-free region. However, the integral is virtually the same, and it is the z-integrals of the functions shown in Figs. 4 and 5 which are needed.

The z-integrals of the flux above 40 keV are given in Table 2. An upper limit to the ratio of the integrals (the scaling factor with energy) is given by the

ratio (20.0 TeV)/(0.875 TeV) = 22.9. The expected value for the scale factor is somewhat lower than this limit; at the higher energies a larger fraction of the cascade is "bled off" into electromagnetic showers because there are more generations of π^0 production. Lindenbaum has suggested that the scaling with energy should be approximately a power law E^m, and the present best value for the exponent is $m = 0.80 \pm 0.10$ [12]. This scaling would predict a ratio of $12.2^{+4.5}_{-3.3}$, in good agreement with the present result.

The area under the preliminary experimental z-distribution is 7.1 cm^{-2}, or 9% higher than the Monte Carlo result after energy correction. The agreement must be regarded as fortuitous, pending pressure gauge calibration and investigation of a number of other experimental corrections.

Table 2
z-integrals of the total neutron flux above 40 keV
as obtained from the December 1986 simulations.

Run	875 GeV ((neutrons cm^{-2})×cm per interacting proton)	20 TeV ((neutrons cm^{-2})×cm per interacting proton)	Ratio
Total	7.70	105.6	13.7
Direct	2.54	35.5	14.0
Albedo*	5.15	70.1	13.6
Albedo + $\frac{1}{2}$ Direct	6.42	87.9	13.7

* Obtained by subtracting the direct flux from the total flux.

There are several ways to understand the integral $\int f(z)dz$. If it is multiplied by the circumference $2\pi\langle r\rangle$, the result is in some sense the "total number of neutrons above 40 keV resulting from one beam-gas collision." In the present case $2\pi\langle r\rangle \approx 635$ cm, so at 875 GeV 4900 "neutrons" are produced, or 5.6 neutrons GeV^{-1}. At 20 TeV, the result is 3.3 GeV^{-1}. This interpretation must be made with caution, however, since the dominant albedo contribution represents multiple counting. For the direct component only, the results are 1.8 GeV^{-1} at 875 GeV and 1.1 GeV^{-1} at 20 TeV. Alternatively, if the constant C as defined above is taken as the machine circumference, then the integral represents the flux at $\langle r\rangle$ averaged over all interaction points around the machine. When this is multiplied by the number of protons lost per second around the ring, it is the desired average flux.

The energy spectrum obtained in the November 1986 runs for 875 GeV incident protons is shown by the histogram in Fig. 6. Before comparing with

experimental results, it should be noted that the simulations provide a *source* spectrum, while the experiment provides the actual source spectrum *as processed through the Bonner sphere spectrometer and unfolding routine.* For comparison purposes, the response of each Bonner sphere must be folded with the calculated spectrum, and then unfolded to obtain the final spectrum. The result of this procedure is shown by the open circles and continuous curve in Fig. 6.* It is typical for such a procedure to broaden a sharp input spectrum, and the slight degradation of the energy at maximum is evidently a consequence of the skewing of the peak to lower energies. The output curve has been arbitrarily normalized to the same area above 40 keV.

For comparison, preliminary spectra from the 1987 experiment are shown in Fig. 7 [2]. The average position of the spectrometer was at 10 m, using the z-origin shown in Fig. 4, so that the scale of the solid curve (N_2 data) should be lower than that of the dotted curve in Fig. 4 by a factor of 2.9. It is in fact lower by 6.4, in spite of the fact that the areas under the z-distributions agree to within 9%. However, as was mentioned in that context, these results are as yet preliminary and uncorrected for a number of effects. The agreement between the simulation and experimental peak positions is quite good for beam-gas cascade origin, while the systematically lower peak energy for "background" production is not understood The shift is particularly puzzling in light of indistinguishable longitudinal distribution shapes for the two sources.

A sampling of more detailed energy spectra from the runs listed in Table 1 is shown in Figs. 8-11. The horizontal scales are very much expanded from those of Figs. 6 and 7, and identical logarithmic vertical scales have been used to facilitate comparison of the 875 GeV and 20 TeV cases. In Figs. 8 and 10, the z bins have been chosen near the intensity maxima, near 9 m from the origin and 1 m from the entrance to the dipole in both cases. Figs. 9 and 11 are similar, except that the z positions were chosen further out in the tail of each distribution. Albedo neutrons dominate more near the peak, and the energy spectra are somewhat softer and very much flattened.

* We thank R. K. Sun of Lawrence Berkeley Laboratory, one of the collaborators on the Tevatron experiment, for carrying out this procedure.

5. Implications for the SSC

The SSC is 83 km in circumference [13]. Each of the two rings contains about 10^{14} protons, and the beam-gas collision lifetime $\tau_{\text{b-g}}$ contribution to the total beam lifetime is of order 100 hr. It is convenient to introduce the dimensionless scaled variables

$$\begin{aligned} \text{Circumference} = C &= 8.3 \times 10^6 C_{83} \text{ cm} \\ \text{Protons/ring} = N_p &= 10^{14} N_{14} \\ \tau_{\text{b-g}} &= 3.6 \times 10^5 \tau_{100} \end{aligned}$$

where, for example, C_{83} is the machine circumference in units of 83 km and τ_{100} is the beam-gas contribution to the lifetime in units of 100 hours. Following the discussion of Sec. 4, one obtains*

$$\begin{aligned} \phi &= \frac{N_p}{C\tau_{\text{b-g}}} \int f(z)dz \\ &= 33.5 \int f(z)dz \; N_{14} C_{83}^{-1} \tau_{100}^{-1} \text{ cm}^{-2}\text{s}^{-1} \; . \end{aligned}$$

The last entry in Table 2 gives the relevant $\int f(z)dz$ as 87.9, so

$$\phi = 2900 \; N_{14} C_{83}^{-1} \tau_{100}^{-1} \text{ cm}^{-2}\text{s}^{-1}$$

for each ring of the SSC.

The time integral of this flux determines the lifetime of electronic components. $\tau_{\text{b-g}}$ is time-dependent for a number of reasons. During fill, acceleration, and tuning, beam losses around the ring substantially reduce the lifetime, contributing substantially to the neutron flux even though they are not technically from beam-gas interactions. During the first several days of SSC operation, the beam-gas lifetime decreases from about 1000 hr to about 20 hr as synchrotron radiation desorbs hydrogen from the cold beam-pipe walls [14]. After a warm (80 K) pumpout, the lifetime is expected to be stable at about 1000 hr during stored-beam conditions. In any case, the relevant fluence is given by

$$2 \times 2900 \; N_{14} C_{83}^{-1} \int \frac{dt}{\tau_{100}(t)} \text{cm}^{-2}$$

where the factor of two is to include both beams. If $(100 \text{ hr})^{-1}$ is a typical average of $1/\tau_{100}$, the neutron exposure in the tunnel will be 0.6×10^{11} cm^{-2} per 10^7 s "SSC year."

* Alternatively, $\phi = 40.5 \int f(z)dz \; I_{70}\tau_{100}$ cm^{-2}s^{-1}, where I_{70} is the beam current in units of 70 mA. The small change in the coefficient has to do with rounding the SSC design parameters as given in the Conceptual Design Report [13].

Acknowledgement

We thank our collaborators participating in the Tevatron tunnel measurements (Fermilab E777) for permission to use preliminary data prior to its publication elsewhere.

Appendix 1. Radiation Damage to Silicon Semiconductors

SSC electronics are damaged primarily by ~ 1 MeV neutrons. Such neutrons scatter (mostly elastically) from silicon atoms. A recoil atom travels a short distance, losing energy primarily by ionization. Near the end of its range, energy loss is dominated by atomic scattering, and the atom dislodges of order 10^3 atoms from their lattice sites as it stops. The result is a combination of vacancies (original locations) and interstitials (final positions), mostly concentrated in an elliptical region near the end of the primary scattered atom's range. Isolated vacancies or interstitials anneal in a relatively short time at ordinary temperatures as the migrating interstitials find vacant lattice sites. More concentrated damage is persistent, and after sufficient irradiation the properties of the silicon are changed to the extent that device operation is impaired.

In this Appendix, the mechanisms leading to the above picture are reviewed. The discussion is intentionally biased toward the radiation composition and spectrum to be expected in the SSC arcs and interaction regions.

As it turns out, damage by ionizing radiation is relatively unimportant. Although an electron (either Compton or direct) can produce a recoil silicon atom, the cross section for displacement by an electron scattering is about twenty times less than that by a neutron at ~ 1 MeV. (See Figs. 9 and 28, Ref. 10.) In addition, the flux of ionizing radiation (electronic and hadronic) in the Tevatron tunnel is substantially less than the neutron flux [1]. Therefore, attention should be focused on the neutron flux, whose spectrum ($d\phi/d(\ln E)$ vs. $\log E$) shows (a) a broad peak at ~ 700 keV neutron kinetic energy, and (b) an increasing flux at very low energies.

The following factors affect the neutron energy dependence of dissociation damage in silicon:

1. The energy transfer must exceed ~ 15 eV to dislodge a silicon atom from its crystal site.
2. If a neutron with kinetic energy T_n scatters through angle θ from an atom

with atomic number A, the kinetic energy T of the recoil atom is given by

$$T/T_n = \frac{4A}{(1+A)^2}\sin^2\theta/2$$
$$(= 0.1332\sin^2\theta/2 \quad \text{for silicon}).$$

The minimum neutron energy which can cause displacement damage in silicon is thus ~ 110 eV. If the scattering is isotropic, then $\langle T\rangle = \frac{1}{2}T_{\max}$, or $0.067\ T_n$ in the case of silicon.

As can be seen from Fig. 6, this threshold implies that the large flux of near-thermal neutrons is effectively harmless.

3. At high energies (e.g. 100 keV) the recoil silicon atom loses energy primarily through ionization, producing few displacements. Near the end of its range (e.g. when its energy has decreased to 10 keV), atomic scattering dominates. For example, for 0.5 MeV incident neutrons only 30% of the silicon atom recoil energy goes into ionization, while for 20 MeV incident particles the fraction has risen to nearly 75% [15]. As a rule of thumb, the energy goes into dislocations for $T < 30$ keV and into ionization at higher energies [10].* For example, the average recoil energy for 1 MeV incident neutrons is ~ 70 keV. The recoiling atom harmlessly loses energy to ionization until it reaches about 30 keV. It then loses energy by displacement, producing (30 keV)/(15 eV) $= O(10^3)$ dislocations.

   A more accurate calculation of this "damage factor" by Messenger is shown in Fig. 12 [16].

   30 keV is the average silicon recoil energy for incident 450 keV neutrons. Below this incident energy, the damage produced per collision is roughly proportional to energy. In combination with the threshold noted above, this means that only the flux under the broad peak in Fig. 6 is effective in producing damage.

4. The DeBroglie wavelength of a 1 MeV neutron is 28×10^{-3} cm, only a factor of 6 or so larger than the radius of a silicon nucleus. Partial waves above $\ell = 0$ thus beginning to be important at this energy, and the angular distribution of scattered particles begins to peak in the forward direction. This decreases the average atomic recoil energy, and therefore the amount of damage produced.

5. The elastic cross section (Fig. 13) of neutrons on ^{28}Si is dominated by a large number of resonances [17]. The average value increases by about an

* More generally, the crossover is at roughly A keV for an atom with atomic number A.

order of magnitude when the energy reaches about 160 keV. In combination with factors mentioned above, this means that the damage cross section effectively "turns on" at this energy.

6. While the relevant cross section is predominantly the elastic cross section at energies below ~ 2 MeV, a variety of other processes† contribute at higher energies, so that the effective dislocation cross section reaches nearly twice the elastic cross section by 10 MeV. (See Fig. 14, taken from Fig. 5 of Ref. 15.)

The combination of all of these factors leads to a relative displacement damage factor as a function of incident neutron energy in silicon, $D(E)$, e.g. as calculated by Messenger [16] or Holmes [18], and most recently by Gabriel *et al.* [19]. This factor, normalized to unity at 1 MeV in accord with (most) convention, is shown in Fig. 15. Given a neutron spectrum $\phi(E)$, the factor relating the damage produced by the measured total flux to the damage done by the same flux of 1 MeV neutrons is given by [16, 20]

$$\int_{E1}^{E2} \phi(E)D(E)dE \Big/ \int_{E1}^{E2} \phi(E)dE \quad .$$

$D(E)$ effectively cuts off the integral in the numerator for energies below 160 keV for the spectra shown in Fig. 6 and in Ref. 1. For values of $E1$ and $E2$ roughly bracketing the peak shown in these figures (say 10 or 100 keV to 20 MeV), the ratio of the two integrals is unity to well within uncertainties in our knowledge of the spectrum or its normalization.

† Si(n,n′)Si, Si(n,p)Al, and Si(n,α)Mg are the most important.

REFERENCES

1. J. B. McCaslin, R-K. S. Sun, and W. P. Swanson; J. J. Elwyn, W. S. Freeman, and P. M. Yurista, SSC Central Design Group Report No. SSC-58 (1986).
2. J. D. Cossairt, A. J. Elwyn, W. S. Freeman, H. Jöstlein, C. D. Moore, and P. M. Yurista; J. B. McCaslin, R-K. S. Sun, and W. P. Swanson; and D. E. Groom, SSC Central Design Group Report, in preparation (1987).
3. R. G. Alsmiller, Jr. *et al.*, "Modifications of the High Energy Transport Code (HETC) and Comparisons with Experimental Results," presented at the ANS Topical Conference on Theory and Practices in Radiation Protection and Shielding, 22-24 April 1987, Knoxville, Tennessee; K. C. Chandler and T. W. Armstrong, "Operating Instructions for the High-Energy Nucleon-Meson Transport Code HETC," Oak Ridge National Laboratory Report ORNL-4744 (1972)
4. M. B. Emmett, "The MORSE Monte Carlo Radiation Transport Code System," Oak Ridge National Laboratory Report ORNL-4972 (February 1975).
5. A. Capella and J. Tran Tanh Van, Z. Phys. C–Particles and Fields **10**, 249-262 (1981).
6. P. A. Aarnio, J. Ranft, and G. R. Stevenson, "A Long Writeup of the FLUKA82 Program," CERN TIS Divisional Report TIS-RP/106-Rev (1984).
7. F. S. Alsmiller, R. G. Alsmiller, Jr., and O. W. Hermann, "Low-Energy Particle Production and Residual Nuclei Production from High-Energy Hadron-Nucleus Collisions," presented at the ANS Topical Conference on Theory and Practices in Radiation Protection and Shielding, 22-24 April 1987, Knoxville, Tennessee.
8. H. W. Bertini, Phys. Rev. **188**, 1711 (1969).
9. R. W. Roussin *et al.*, "VITAMIN-E: A Coupled 174-Neutron, 38-Gamma-Ray Multigroup Cross-Section Library for Deriving Application-Dependent Working Libraries for Radiation Transport Calculations," available from the Radiation Shielding Information Center, Engineering Physics & Mathematics Division, Oak Ridge National Laboratory, as DLC-113/ VITAMIN-E.
10. J. E. Gover, and J. R. Srour, "Basic Radiation Effects in Nuclear Power Electronics Technology, Sandia Report SAND85-0776 (1986).

11. H. T. Edwards, *Ann. Rev. Nucl. Part. Sci.* **35**, 605-660 (1985), and F. T. Cole, M. R. Donaldson, D. A. Edwards, H. T. Edwards, and P. F. M. Koehler, editors, "A Report on the Design of the Fermi National Accelerator Laboratory Superconducting Accelerator," Fermilab (1979).

12. R. H. Thomas and G. R. Stevenson, *Radiological Safety Aspects of the Operation of Proton Accelerators,* IAEA Technical Report Series (1987) (to be published).

13. "Superconducting Super Collider Conceptual Design," SSC Central Design Group Report SSC-SR-2020 (1986).

14. D. Bintinger, P. Limon, H. Jöstlein, and D. Trbojevic, "Status of the SSC Photodesorption Experiment," SSC Central Design Group Report SSC-102(1986).

15. H. J. Stein, J. App. Phys. **38** 204-210 (1967).

16. G. C. Messenger, IEEE Trans. Nucl. Sci., pp. 53-74, April 1965.

17. "Neutron Cross Sections, "Brookhaven National Laboratory Report BNL 325 (1976).

18. R. R. Holmes, "Energy Dependence for Carrier Removal and Lifetime Damage by Fast Neutrons in Silicon," Bell Telephone Laboratories Weapons Effects Studies, Vol. II, October 1, 1970.

19. T. A. Gabriel, J. D. Amburgey, and N. M. Greene, Nucl. Sci. Eng. **61**, 21-32 (1976); T. A. Gabriel and B. L. Bishop, "Radiation Damage in Silicon Due to Albedo Neutrons Emitted from Hadron Beam Dumps (Iron and Uranium)," presented at the ANS Topical Conference on Theory and Practices in Radiation Protection and Shielding, 22-24 April 1987, Knoxville, Tennessee.

20. J. M. McKenzie, IEEE Trans. Nucl. Sci., pp. 18-24, August 1973.

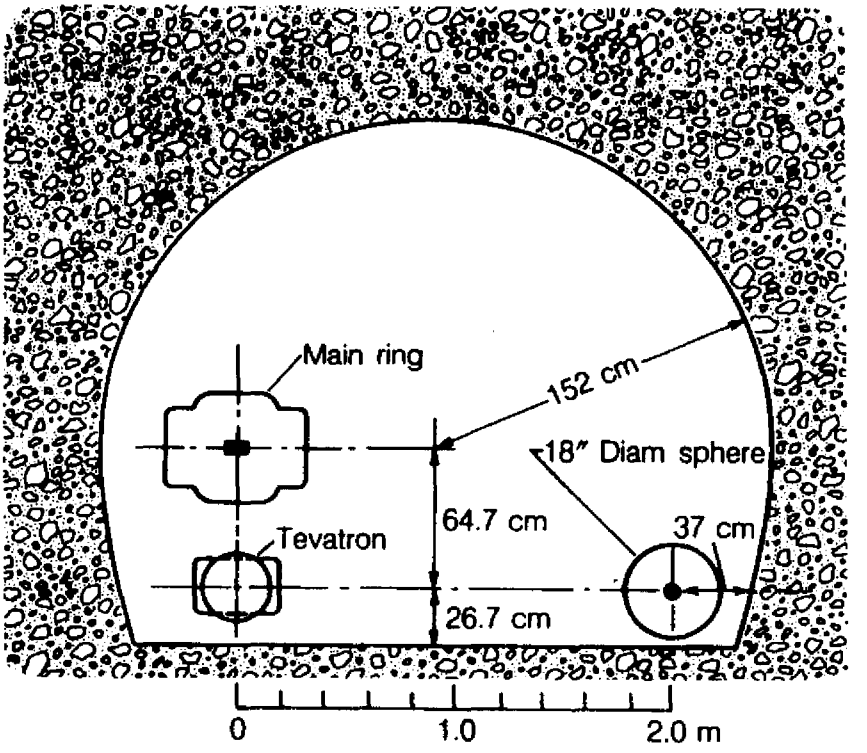

1. Cross section of the Tevatron tunnel, showing relevant dimensions and the placement of the neutron flux measuring equipment. (From Ref. 1.)

SSC Tunnel Model
(not to scale)

ORNL 12/86

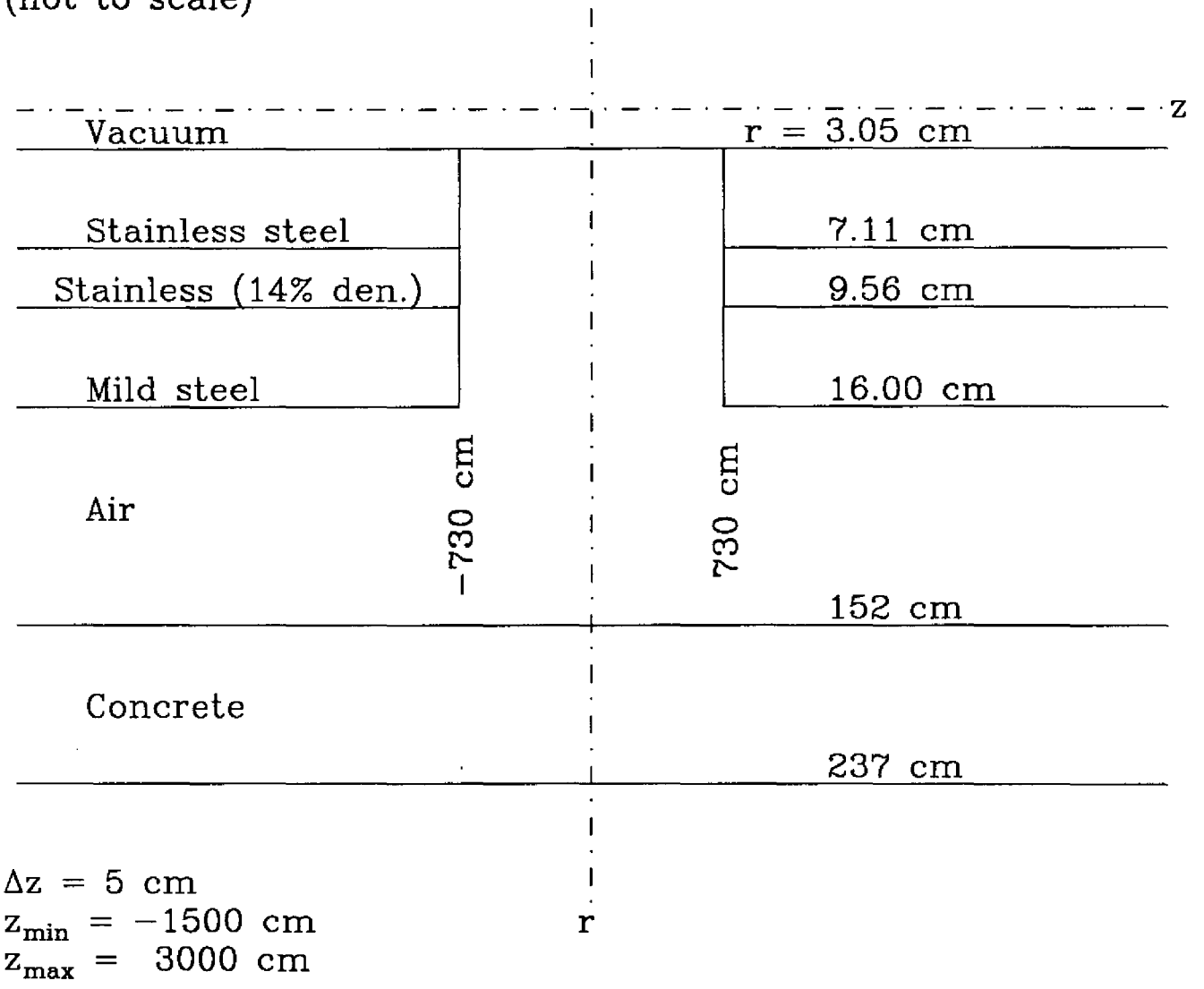

$\Delta z = 5$ cm
$z_{min} = -1500$ cm
$z_{max} = 3000$ cm

2. ORNL cylindrically symmetric model of the Tevatron tunnel and magnet along the *z* direction, showing dimensions and assumed compositions. The dipole-free region (±730 cm) represents the A17 warm section.

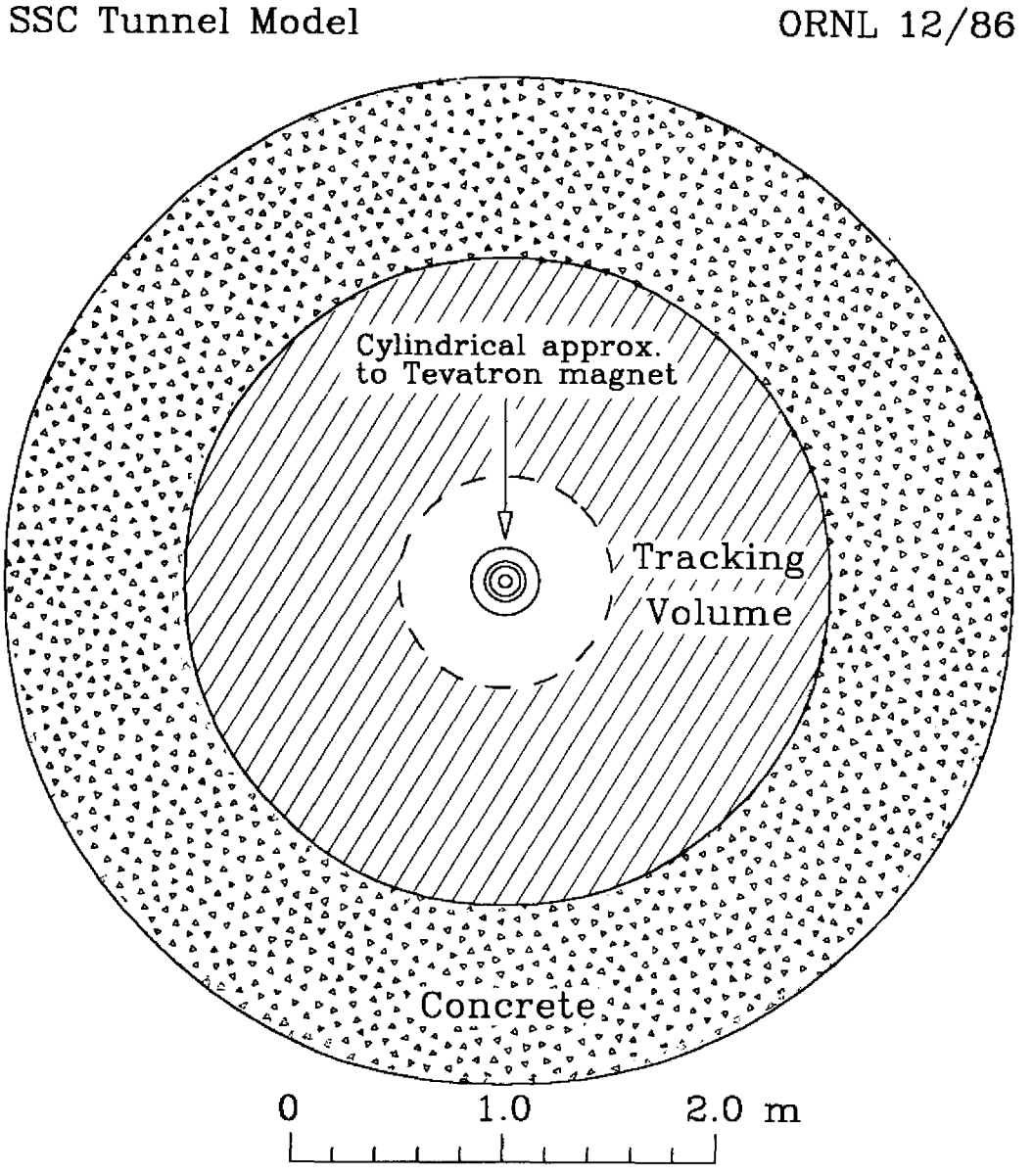

3. Transverse cut of the ORNL model to the same scale as Fig. 1. Flux is obtained from neutron path lengths in the "tracking volume."

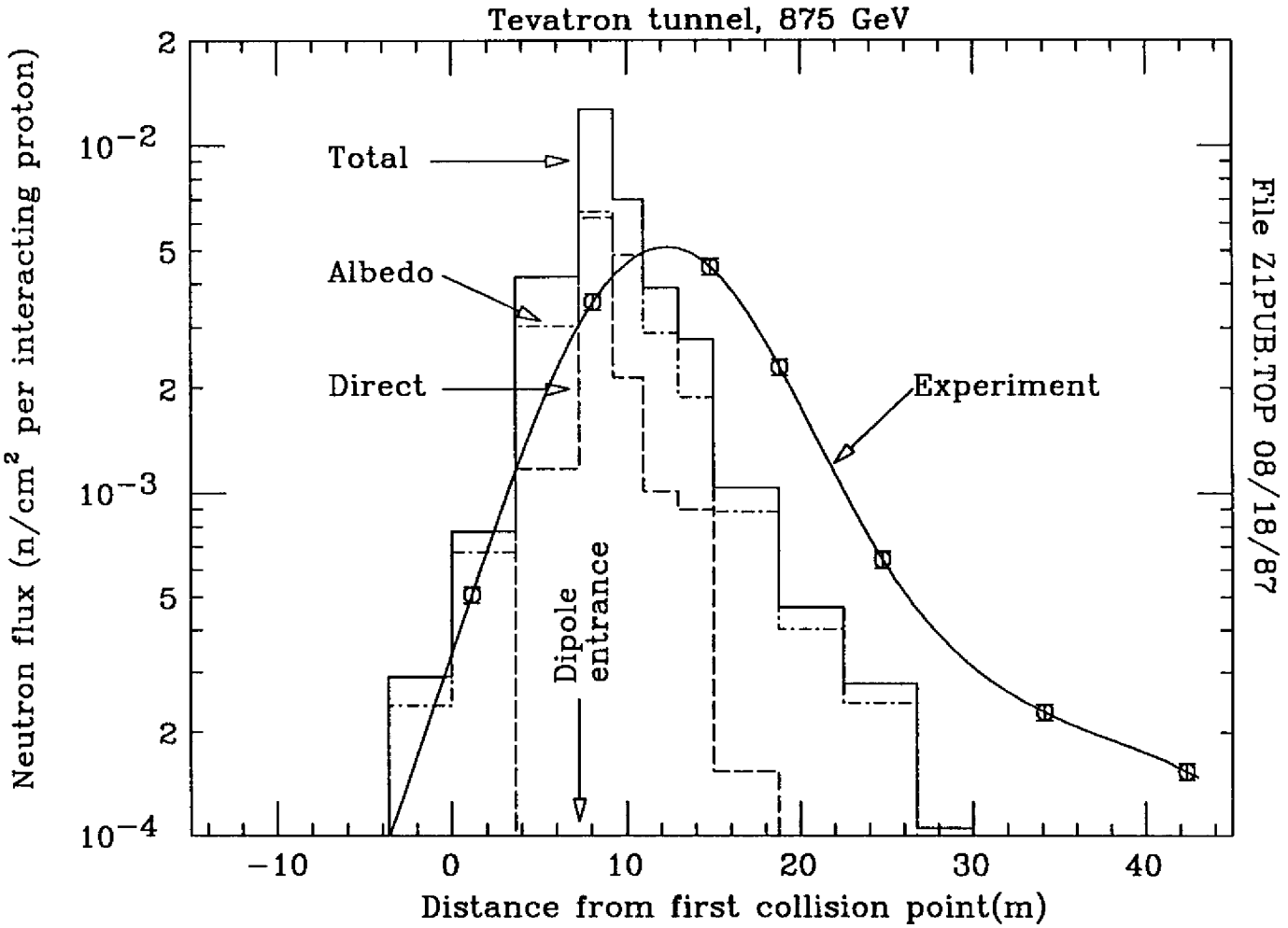

4. Calculated longitudinal distributions of neutron flux ($E > 40$ keV) in the Tevatron tunnel for 875 GeV incident proton energy (histograms), and measured distribution from Ref. 2.

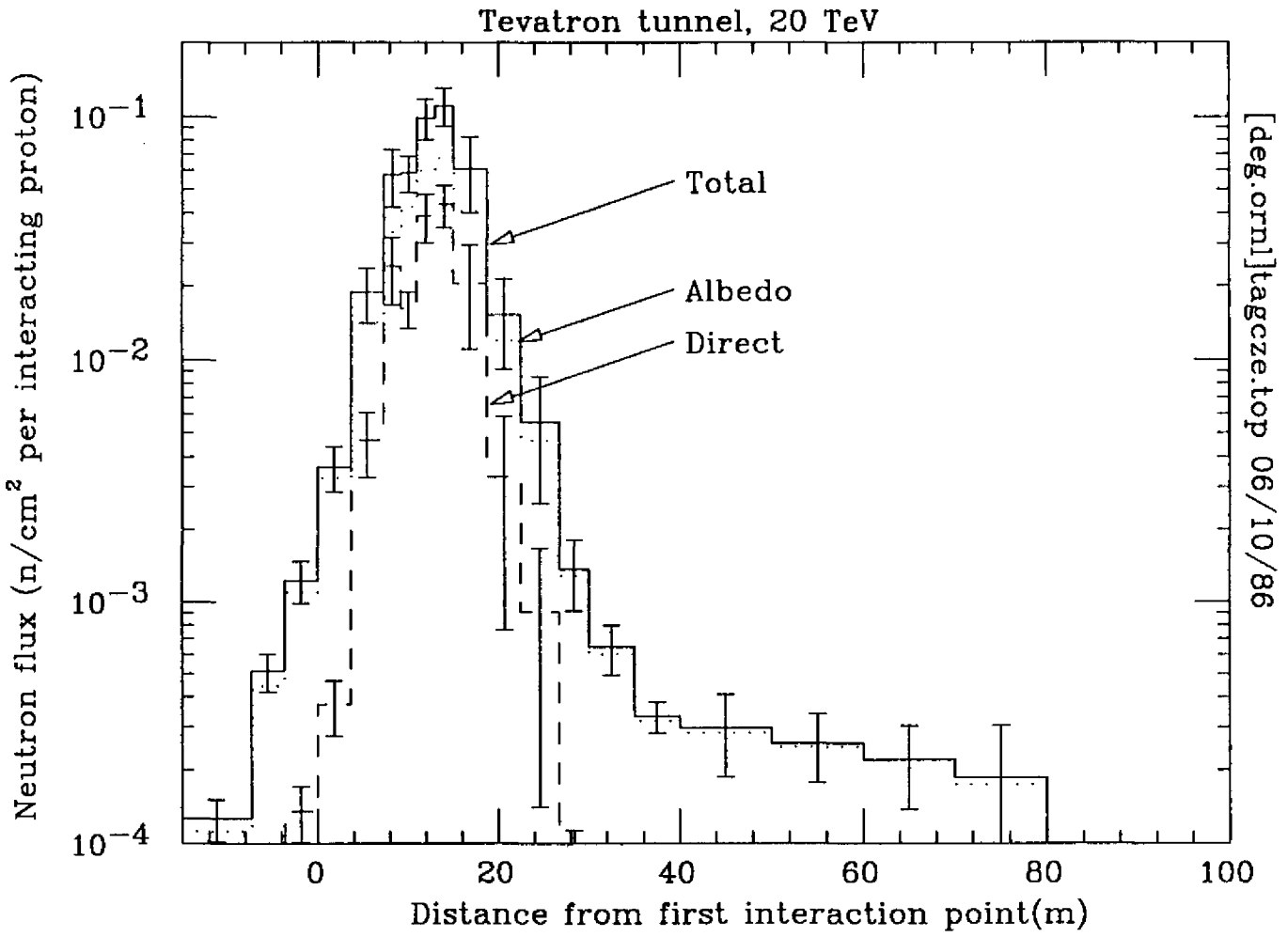

5. Calculated longitudinal distributions of neutron flux ($E > 40$ keV) in the Tevatron tunnel for 20 TeV incident proton energy.

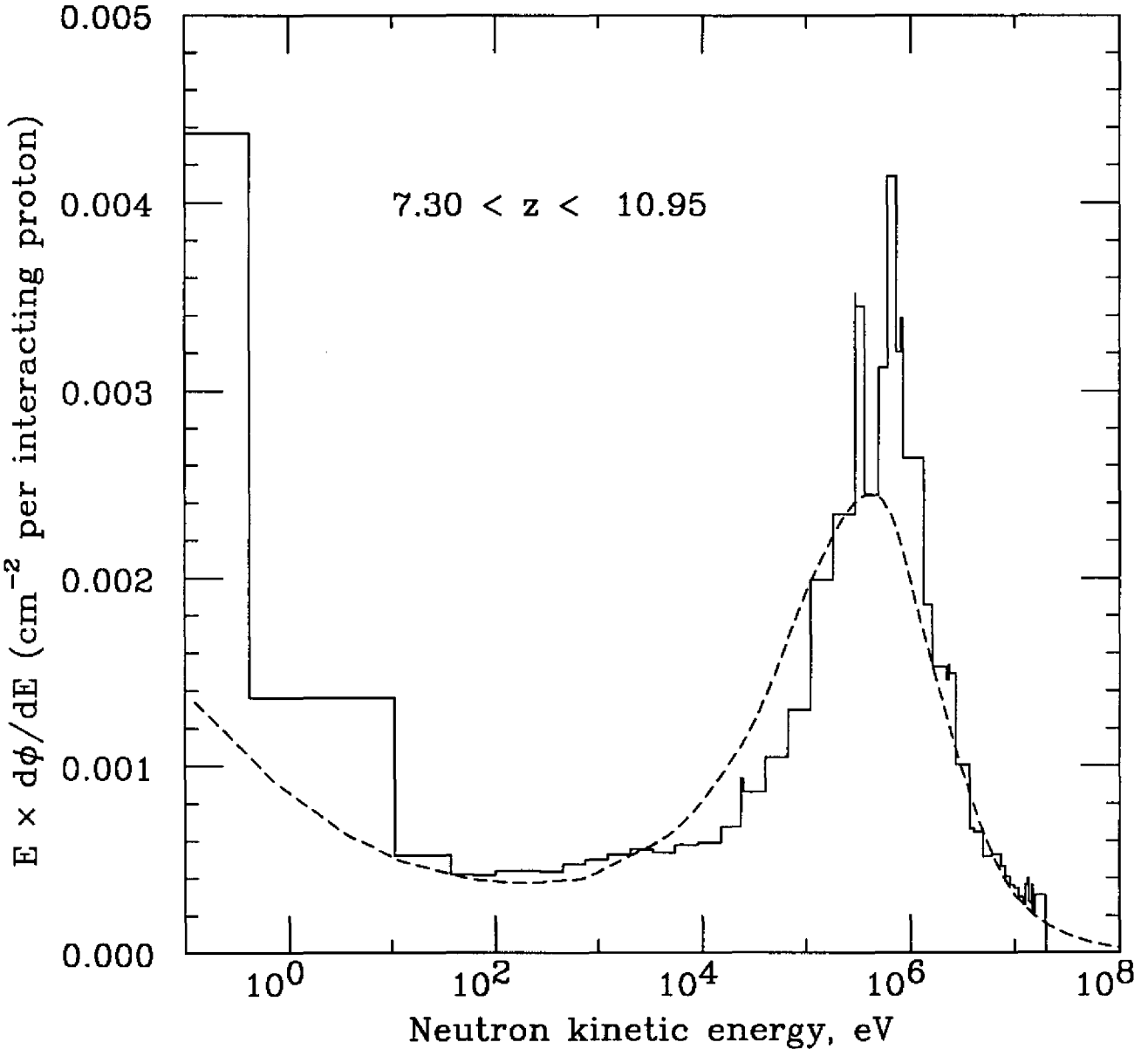

6. Calculated energy spectrum of the total neutron flux near the maximum of the longitudinal distribution in an 875 GeV simulation (histogram), and the result of processing these data through the Bonner sphere spectrometer and unfolding program LOUHI (smooth curve.)

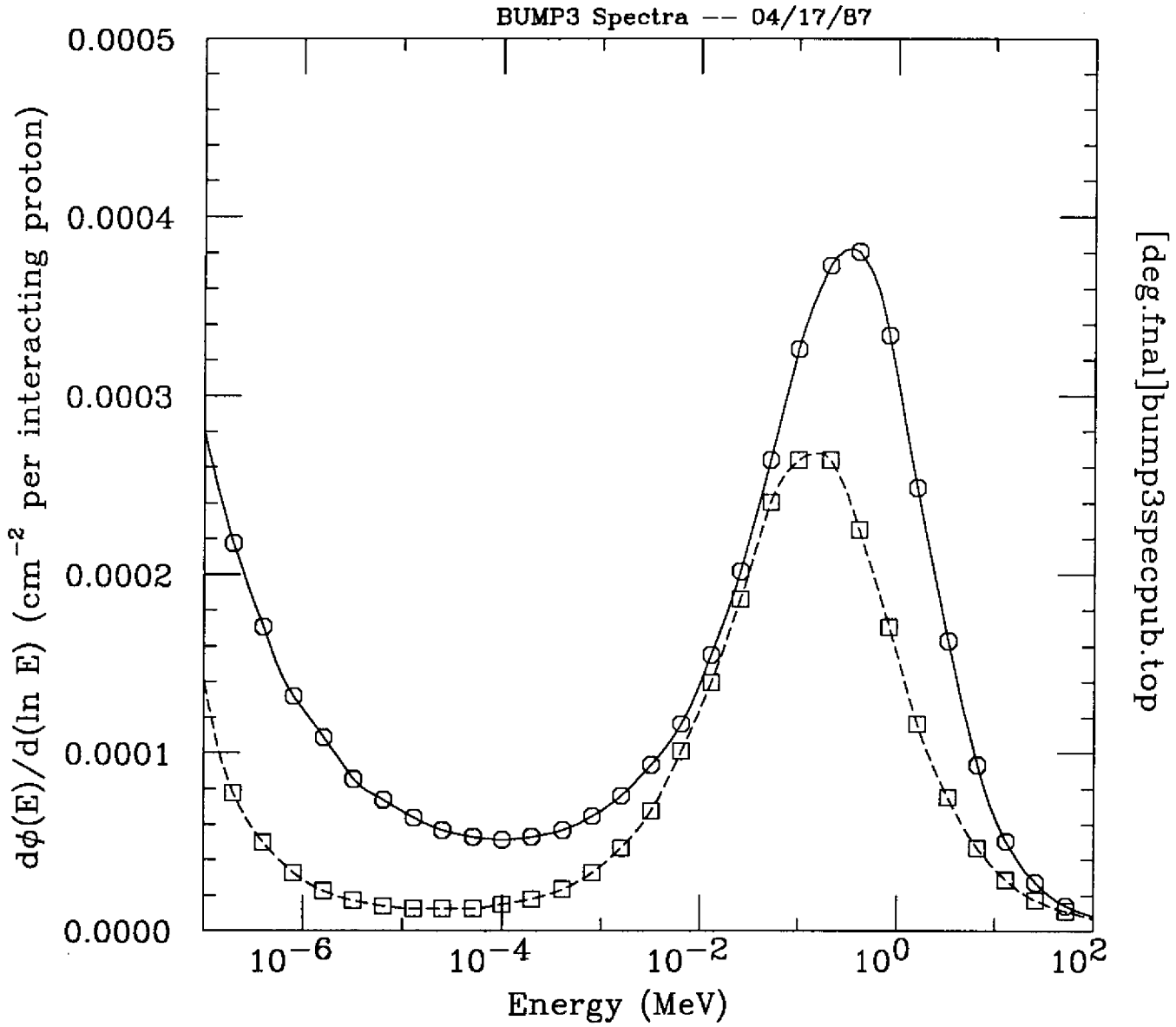

7. Preliminary neutron spectra observed near the tunnel wall near the Tevatron ring in 1987[2]. The solid curve is for production from N_2 in the warm section, and the dashed curve for background of unknown origin (at extrapolated zero pressure.) Normalization of the solid curve is absolute for $z = 10$ m pending pressure gauge calibration and other corrections, while that of the dashed curve is of necessity arbitrary. The Bonner sphere spectrometer data were unfolded using program LOUHI[1]).

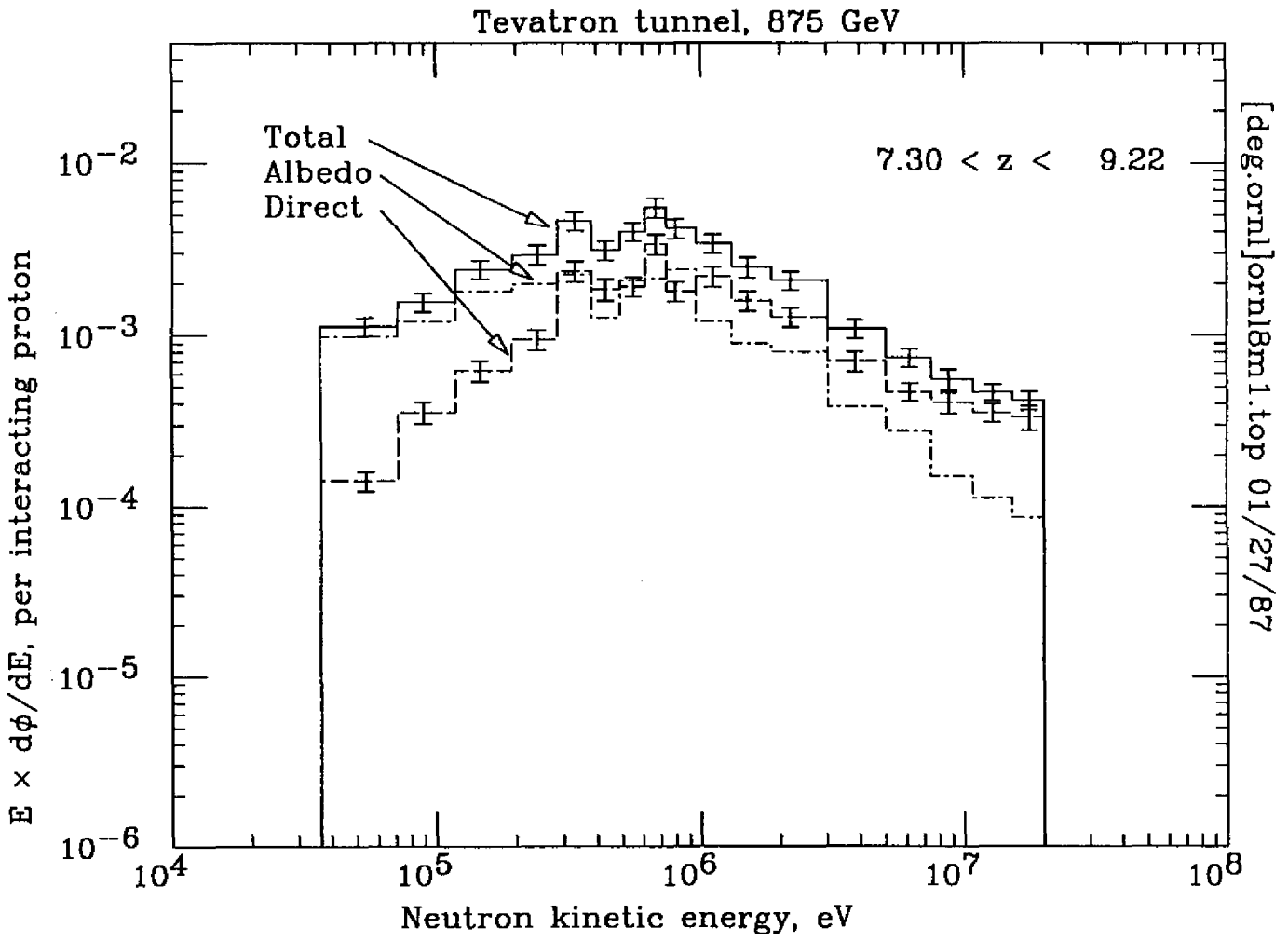

8. Calculated energy spectrum near maximum of the z distribution for 875 GeV incident protons. The albedo contribution is obtained by subtracting the direct flux (no tunnel walls) from the total flux (with tunnel walls). Errors on the difference are somewhat larger than shown for the other histograms, but are deleted for clarity.

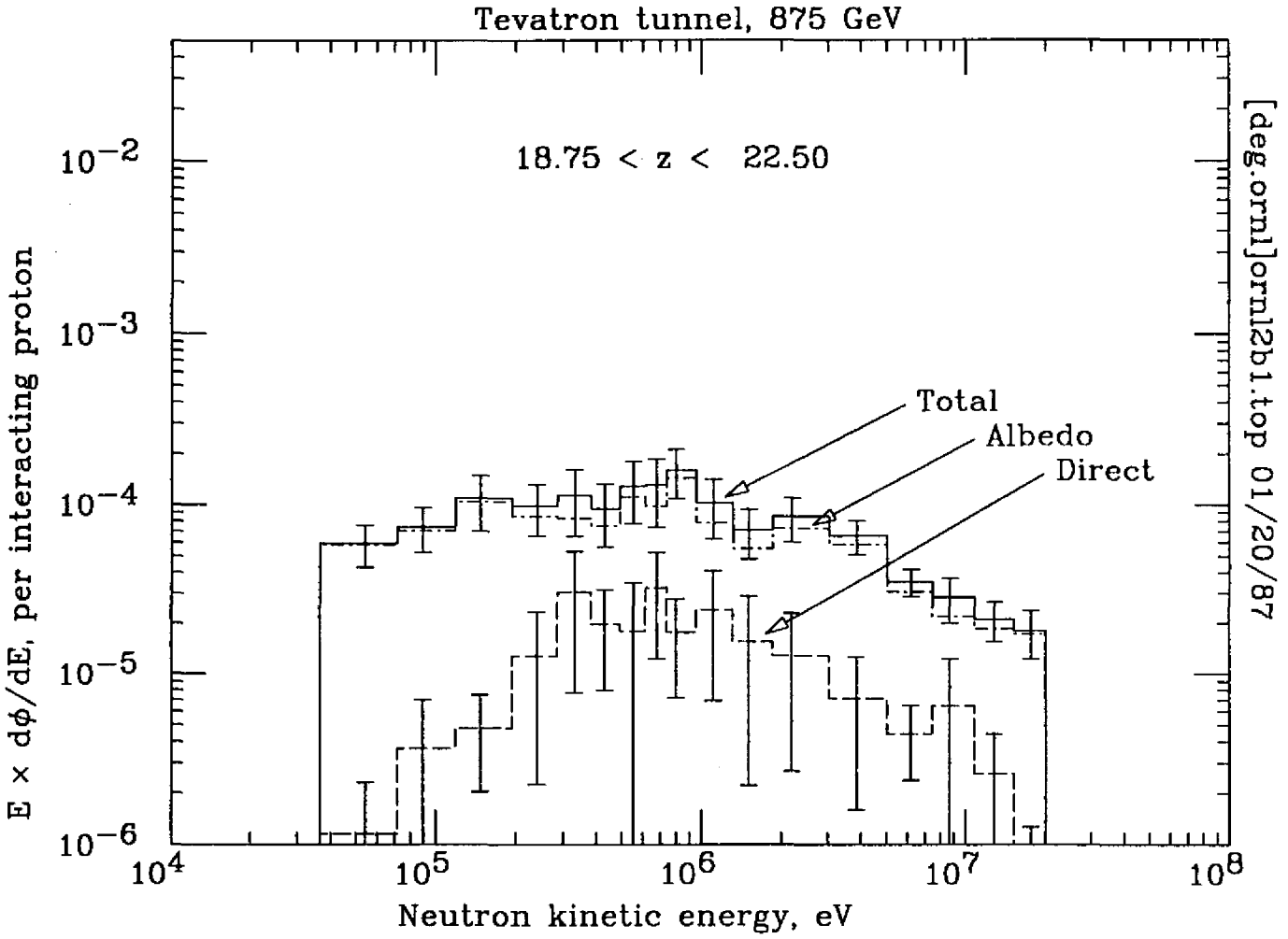

9. Calculated energy spectrum in the tail of the z distribution for 875 GeV incident protons. The albedo contribution is obtained by subtracting the direct flux (no tunnel walls) from the total flux (with tunnel walls).

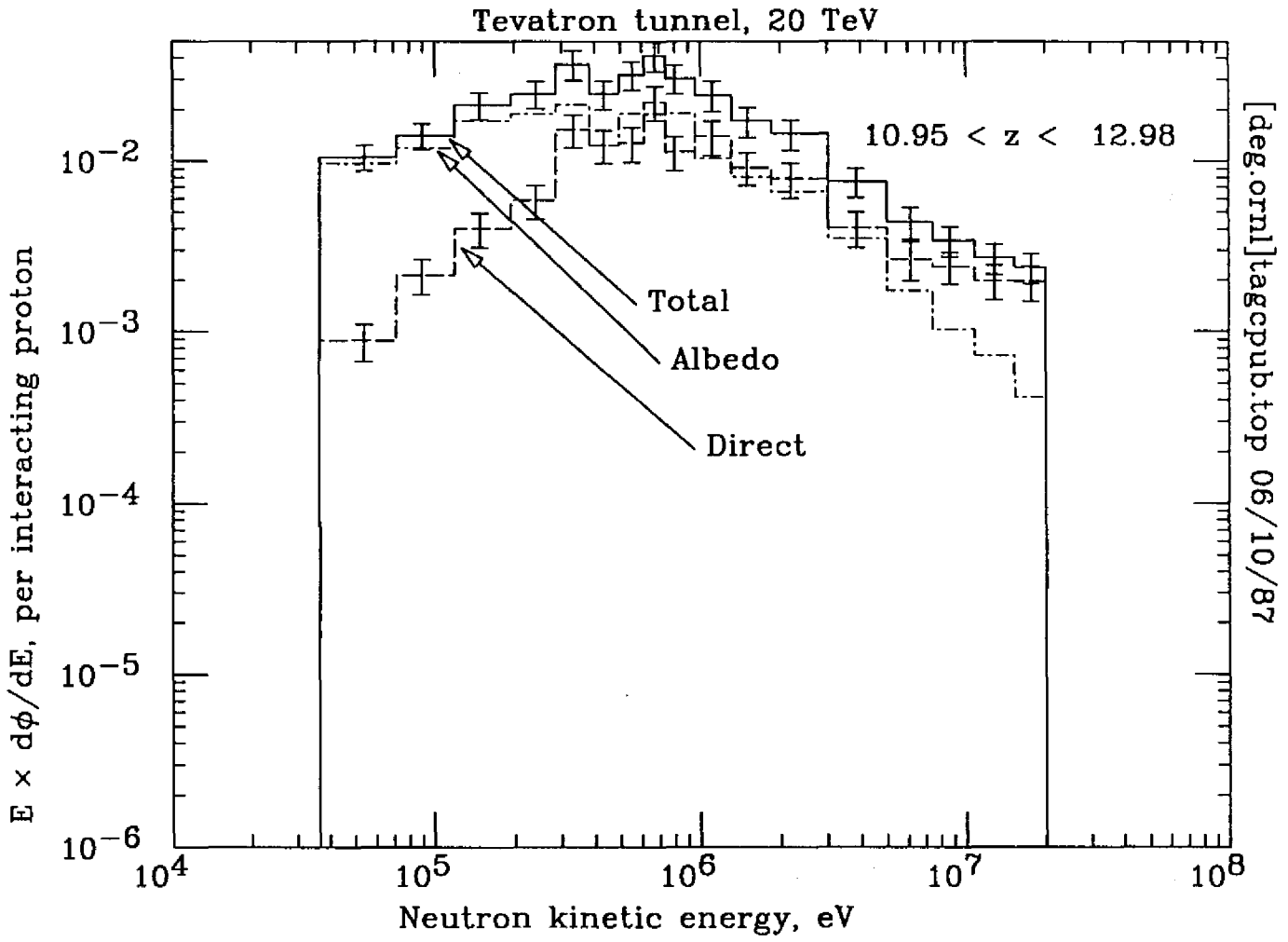

10. Calculated energy spectrum near maximum of the z distribution for 20 TeV incident protons. The albedo contribution is obtained by subtracting the direct flux (no tunnel walls) from the total flux (with tunnel walls). Errors on the difference are somewhat larger than shown for the other histograms, but are deleted for clarity.

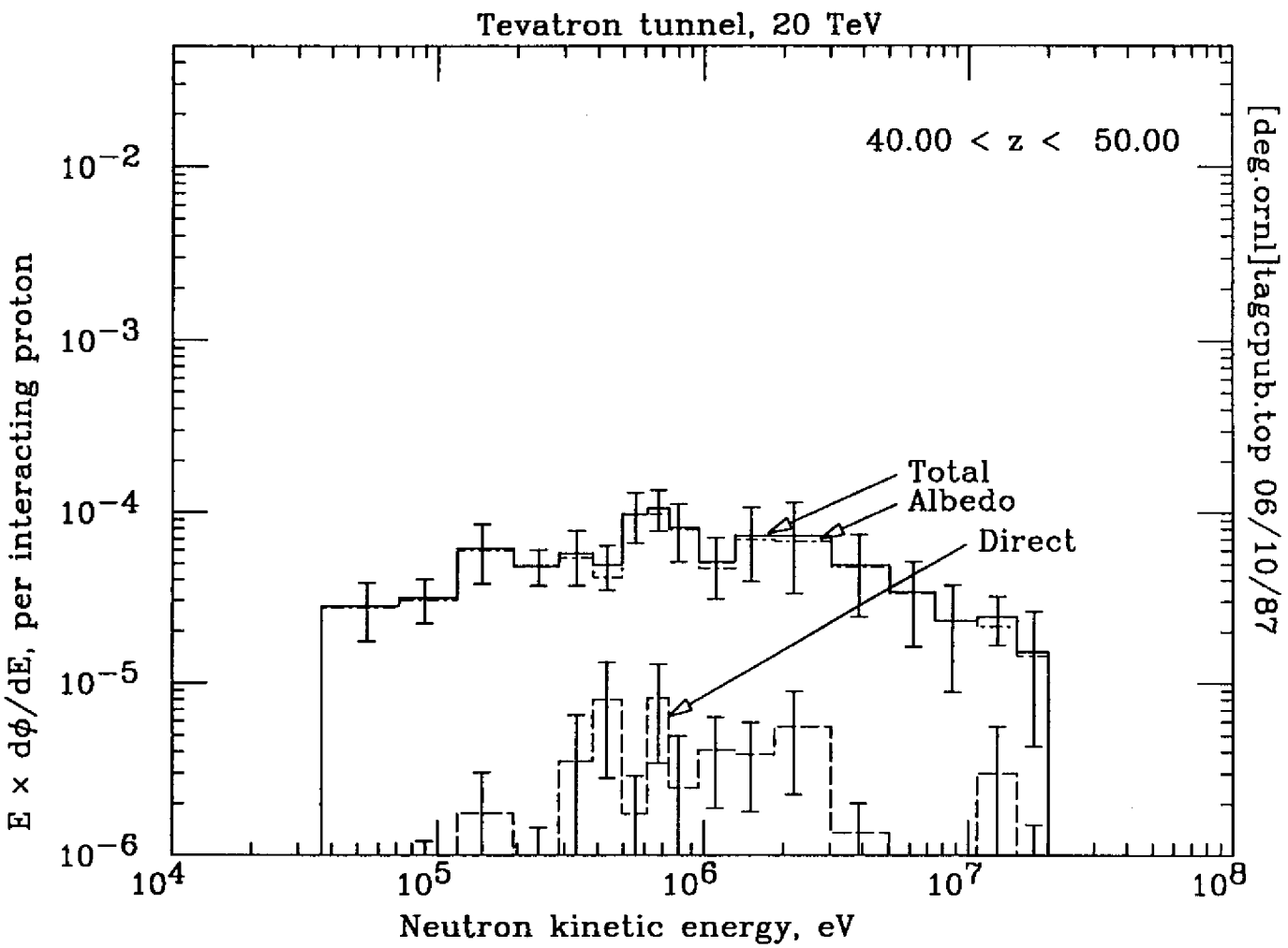

11. Calculated energy spectrum in the tail of the z distribution for 20 TeV incident protons. The albedo contribution is obtained by subtracting the direct flux (no tunnel walls) from the total flux (with tunnel walls).

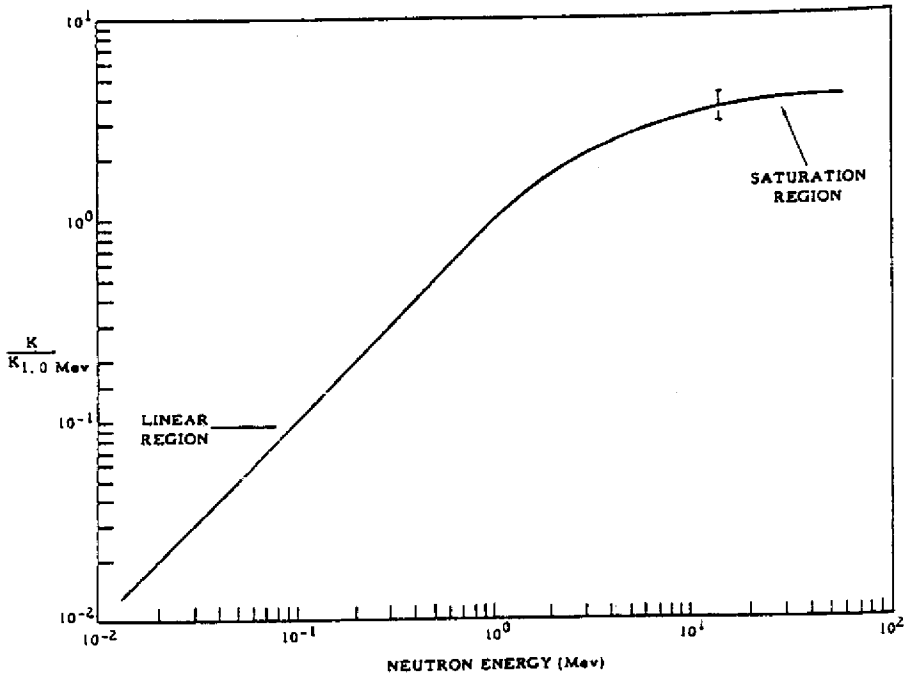

12. Lifetime damage factor as a function of neutron energy for silicon, normalized to unity at 1 MeV.

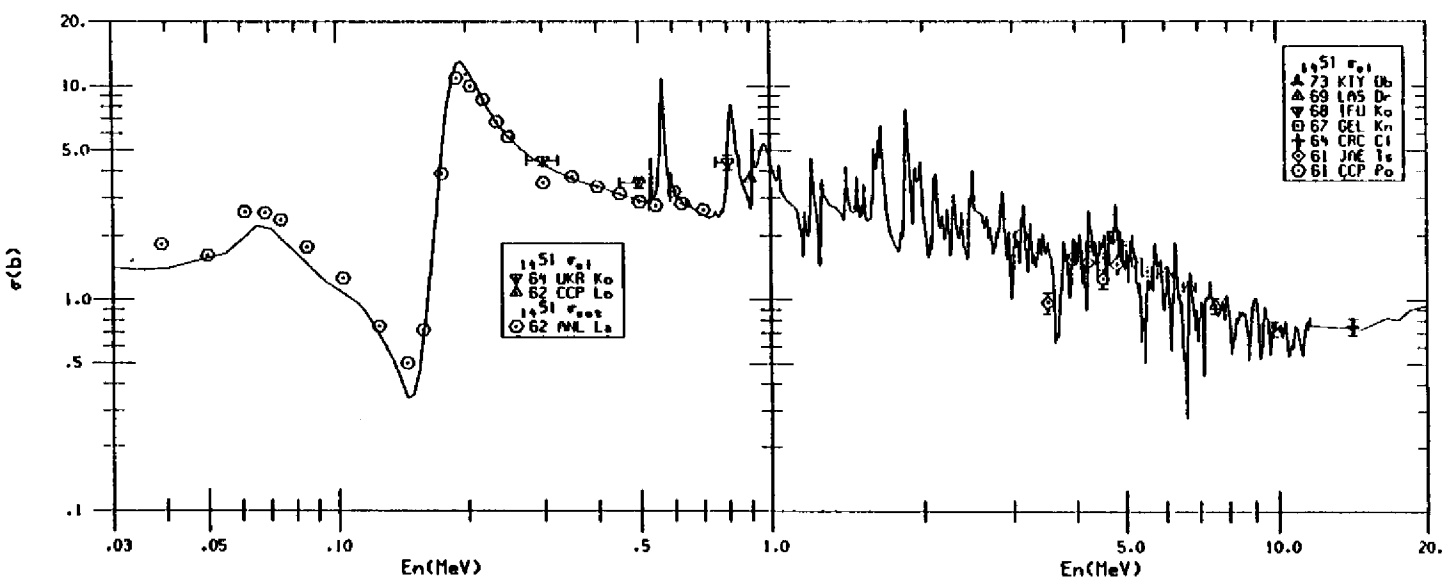

13. Elastic cross section for neutrons on ^{28}Si [18].

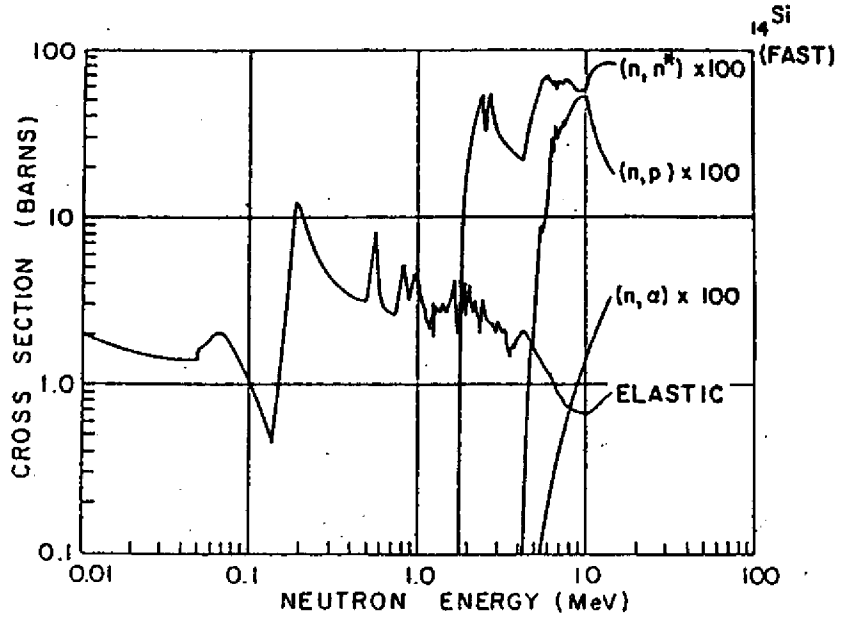

14. Contributions to the displacement cross section for neutrons on ^{28}Si, from Stein [16].

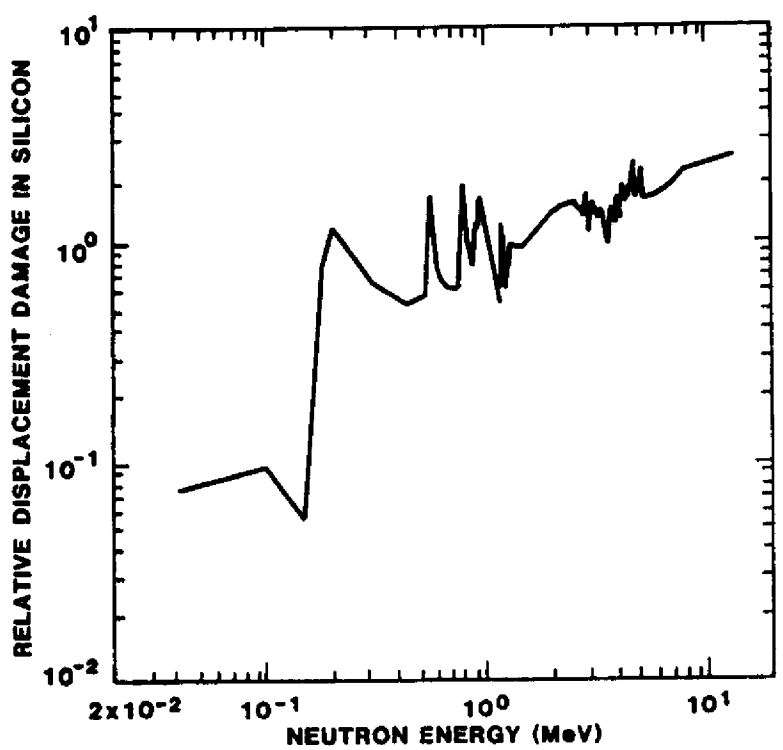

15. Displacement damage coefficient for neutrons on ^{28}Si, normalized to unity at 1 MeV, as given by Gover and Srour [9]. The original source is probably Holmes [19].